5007

A comparison of dynamic and static B0 mapping approaches for correction of CEST MRI at 7T

Esau Poblador Rodriguez[1], Philipp Moser[1], Barbara Dymerska[2], Simon Robinson[1], Benjamin Schmitt[3], Andre van der Kouwe[4], Stephan Gruber[1], Siegfried Trattnig[1,5], and Wolfgang Bogner[1]

[1]High Field MR Centre, Department of Biomedical Imaging and Image-guided Therapy, Medical University of Vienna, Vienna, Austria, [2]Medical Physics and Bioengineering, University College London, London, United Kingdom, [3]Siemens Healthineers, Sydney, Australia, [4]Athinoula A. Martinos Center for Biomedical Imaging, Department of Radiology, Massachusetts General Hospital, Harvard Medical School, Boston, MA, United States, [5]Christian Doppler Laboratory for Clinical Molecular MR Imaging, Vienna, Austria

Synopsis

In contrast to established static B_0 correction approaches which assume an invariant static field during a CEST MRI acquisition, we propose three methods which can track and compensate temporal B_0 fluctuations by shifting each Z-spectral point separately before MTR_{asym} analysis. We show the benefit of the proposed dynamic methods in comparison to three established static approaches by assessing their performance in the absence/presence of an induced frequency drift. In addition, we investigate the reliability and reproducibility of CEST MRI at ultra-high field (7T) by evaluating the drift's impact on the B_0-corrected MTR_{asym} maps in the brains of five healthy volunteers.

Introduction

Chemical **E**xchange **S**aturation **T**ransfer (CEST) MRI benefits from ultra-high field due to increased spectral resolution. Local magnetic field inhomogeneities, δB_0, are more severe, however, complicating CEST quantification[1]. Static B_0-correction techniques are prone to errors since they assume negligible temporal B_0-fluctuations arising from system instabilities (such as frequency drifts) or involuntary subject movement. We propose and compare the in vivo performance of three different dynamic B_0-correction methods for CEST MRI which should lead to more reliable MTR_{asym} maps than three established static B_0-correction approaches in the presence of B_0-instabilities.

Methods

The three δB_0 mapping approaches for static CEST correction were:

(A) CEST-minZ: δB_0 from the minimum of the interpolated Z-spectra (intrinsic)[2]

(B) WASSR: δB_0 from high spectrally resolved Z-spectra without fat suppression (pre-scan)[1]

(C) GRE-2TE: δB_0 from a dual-echo gradient echo (GRE) readout reference scan (pre-scan)[3]

The three proposed B_0 tracking approaches for dynamic CEST correction were:

(D) CEST-GRE-2TE: $\delta B_0(t)$ from a dual-echo GRE readout which replaces the single-echo GRE readout after the CEST-labeling module (intrinsic)[4]

(E) CEST-GRE-1TE: $\delta B_0(t)$ from a single-echo GRE readout after the CEST-labeling module. Additionally, coil phase offset maps need to be determined (intrinsic/pre-scan)[5;6]

(F) NAV-EPI-2TE: $\delta B_0(t)$ from a dual-echo multi-shot EPI readout that is interleaved with the CEST sequence (interleaved navigator)[7;8]

The study was performed on a whole-body 7T MR system (Magnetom, Siemens) with a ^{1}H 32-channel head coil (Nova Medical). The 2D sequences had a resolution of 2.1x2.1x6.0mm³ for which image acquisition/analysis parameters were matched (details in Table 1). Image processing, coil combination, B_0 map calculation and ROIs statistics were conducted in MATLAB (MathWorks). B_0-correction and asymmetric magnetic transfer ratio (MTR_{asym}) analysis were performed voxel wise.

Initial phantom tests were performed to evaluate the consistency of the B_0 mapping among the different methods and to stablish their dependency on the CEST-labeling module.

The impact of the method of B_0 determination on the MTR_{asym} was assessed in five healthy volunteers. To show the performance of the dynamic compensation methods versus the static methods in the presence of scanner instabilities, a ~4Hz/min frequency drift was induced during the CEST re-scan (protocol flow in FIG.1). This is consistent with previous reported drifts at 3T[9-11].

Results

The dynamic correction methods successfully tracked the B_0 evolution to independently correct each Z-spectral point before MTR_{asym} analysis. The intrinsic dynamic methods CEST-GRE-2TE and CEST-GRE-1TE were not corrupted by the RF saturation prior to the CEST readout for $\Delta\omega \approx > |0.24|$ppm. FIG.2 shows the effect of the B_0 determination on the corrected MTR_{asym} curves among the different correction methods. In the presence of an induced ~4Hz/min drift, the established static methods resulted in severely underestimated (~1/3 for CEST-minZ) or overestimated (~3 times for WASSR and GRE-2TE) ratios compared to the stable case. CEST-minZ estimated B_0 approximately at the end of the CEST scan ($\delta B_{0(12min)} \approx 48$Hz) in contrast to the pre-scans WASSR and GRE-2TE ($\delta B_{0(0min)} \approx 0$Hz).

The resulted color-coded MTR_{asym} maps are presented in FIG.3. Among the dynamic correction methods, NAV-EPI-2TE and CEST-GRE-2TE provided closest B_0-corrected contrasts between the two CEST acquisitions (stable conditions VS induced drift). CEST-GRE-1TE showed some deviations, but was still better than all static methods.

To investigate the CEST scan-rescan reproducibility, a comparison among five healthy volunteers was performed. The results provided by NAV-EPI-2TE, presented in FIG.4, show highly consistent MTR_{asym} maps. CEST-GRE-2TE achieved similar uniform results among volunteers with the exception of frontal and periventricular discrepancies in volunteer V2.

Discussion and Conclusion

The current study focused on the MTR_{asym} integration range $\Delta\omega=\pm[0.24\text{-}1.18]$ppm, to test the performance of the proposed correction methods for the most challenging frequencies due to the high slope of the Z-spectrum[1].

The proposed dynamic method CEST-GRE-2TE tracks the B_0 field intrinsically from a dual-echo CEST scan requiring no additional measurements, making it widely applicable. CEST-GRE-1TE shortens the measurement time by allowing a single-echo CEST scan, at the expense of a negligible ~1s long pre-scan. The implementation of NAV-EPI-2TE is more complex since it requires interleaved B_0 maps via a navigator, but it is completely insensitive to the RF saturation applied for CEST-labeling.

The proposed dynamic methods could be additionally combined with real-time motion correction by extending the navigator to 3D as previously shown for MRI and MRSI [7;8;12;13]. Such techniques will be assessed in further work to, on top of B_0-instabilities, readily correct for motion-induced δB_0.

This study provides an excellent basis for reliable clinical CEST MRI in presence of temporarily fluctuating B_0-inhomogeneities, offering more accurate water resonance determination, avoiding the need of lengthy pre-scans (required for WASSR) and shortening the measurement time by allowing the use of fewer Z-spectral points (as required for CEST-minZ).

Acknowledgements

This material is based upon work supported by Christian Doppler Laboratory for Clinical Molecular MRI and the Austrian Science Fund (FWF) under Grant KLI-718.

Special gratitude to Vladimir Mlynarik for his guidance and assistance.

References

1. Kim M, Gillen J, Landman BA, Zhou J, van Zijl PC. 2009. Water saturation shift referencing (wassr) for chemical exchange saturation transfer (cest) experiments. Magn Reson Med. 61(6):1441-1450.

2. Zaiss M, Schmitt B, Bachert P. 2011. Quantitative separation of cest effect from magnetization transfer and spillover effects by lorentzian-line-fit analysis of z-spectra. J Magn Reson. 211(2):149-155.

3. Kawanaka A, Takagi M. 1986. Estimation of static magnetic field and gradient fields from nmr image. Journal of Physics E: Scientific Instruments. 19(10): 871.

4. Visser E, Poser BA, Barth M, Zwiers MP. 2012. Reference-free unwarping of epi data using dynamic off-resonance correction with multiecho acquisition (docma). Magn Reson Med. 68(4):1247-1254.

5. Robinson S, Grabner G, Witoszynskyj S, Trattnig S. 2011. Combining phase images from multi-channel rf coils using 3d phase offset maps derived from a dual-echo scan. Magn Reson Med. 65(6):1638-1648.

6. Dymerska B, Poser BA, Barth M, Trattnig S, Robinson SD. 2018. A method for the dynamic correction of b0-related distortions in single-echo epi at 7t. NeuroImage. 168:321-331.

7. Hess AT, Tisdall MD, Andronesi OC, Meintjes EM, van der Kouwe AJ. 2011. Real-time motion and b0 corrected single voxel spectroscopy using volumetric navigators. Magn Reson Med. 66(2):314-323.

8. Bogner W, Hess AT, Gagoski B, Tisdall MD, van der Kouwe AJ, Trattnig S, Rosen B, Andronesi OC. 2014. Real-time motion- and b0-correction for laser-localized spiral-accelerated 3d-mrsi of the brain at 3t. NeuroImage. 88:22-31.

9. Harris AD, Glaubitz B, Near J, John Evans C, Puts NA, Schmidt-Wilcke T, Tegenthoff M, Barker PB, Edden RA. 2014. Impact of frequency drift on gamma-aminobutyric acid-edited mr spectroscopy. Magn Reson Med. 72(4):941-948.

10. Rowland BC, Liao H, Adan F, Mariano L, Irvine J, Lin AP. 2017. Correcting for frequency drift in clinical brain mr spectroscopy. Journal of neuroimaging : official journal of the American Society of Neuroimaging. 27(1):23-28.

11. Lee CY, Choi IY, Lee P. 2018. Prospective frequency correction using outer volume suppression-localized navigator for mr spectroscopy and spectroscopic imaging. Magn Reson Med.

12. Hess AT, Andronesi OC, Tisdall MD, Sorensen AG, van der Kouwe AJ, Meintjes EM. 2012. Real-time motion and b0 correction for localized adiabatic selective refocusing (laser) mrsi using echo planar imaging volumetric navigators. NMR in biomedicine. 25(2):347-358.

13. Alhamud A, Taylor PA, van der Kouwe AJ, Meintjes EM. 2016. Real-time measurement and correction of both b0 changes and subject motion in diffusion tensor imaging using a double volumetric navigated (dvnav) sequence. NeuroImage. 126:60-71.

Figures

		TR [ms]	TE1 [ms]	TE2 [ms]	BW [Hz/Px]	FA [º]	Echo Train Length	Miscellaneous
STATIC	CEST-minZ	9.5	1.74	-	780	6	128	Ts=700 ms, $B1^{rms}$=2.0 µT, Δω=0.08 ppm
	WASSR	9.5	1.74	-	780	6	128	Ts=100 ms, $B1^{rms}$=0.2 µT, Δω=0.013ppm
	GRE-2TE	9.5	1.74	5.16	780	6	128	
DYNAMIC	CEST-GRE-2TE	9.5	1.74	5.16	780	6	128	Ts=700 ms, $B1^{rms}$=2.0 µT, Δω=0.08 ppm
	CEST-GRE-1TE	9.5	1.74	-	780	6	128	Ts=700 ms, $B1^{rms}$=2.0 µT, Δω=0.08 ppm
	NAV-EPI-2TE	15	5.4	9.0	2442	5	4	

Table 1. Summary of relevant parameters for each of the B_0 acquisition methods evaluated. Static methods correct for B_0 inhomogeneities by shifting the entire Z-spectrum and hence assuming no drift or fluctuation in the static field throughout the CEST measurement. Dynamic methods, on the other hand, track its temporal B_0 evolution to shift each Z-value (at certain saturation frequency offset $\Delta\omega$) independently.

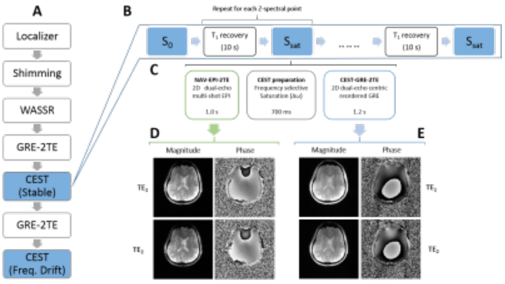

FIG. 1: An overview of the experimental protocol followed to compare 6 B_0-correction methods (A). Scheme of the CEST measurement (B), in which a delay for T1 recovery of water signal is interleaved with S_0 and S_{sat} acquisitions, each of them consisting of three blocks (C): an EPI navigator with dual-echo readout scan generating magnitude and phase images per echo time (D); a CEST-labeling period in which the magnetization is saturated by a train of Gaussian pulses at a sweeping frequency offset $\Delta\omega$; and a GRE with dual-echo readout scan generating magnitude and phase images per echo time (E).

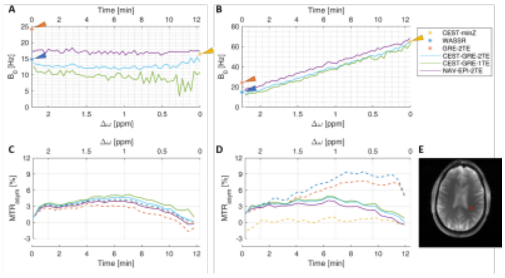

FIG. 2: Impact of a ~4Hz/min frequency drift within an ROI for volunteer V1 (E). ROI-averaged B_0 tracking without (A) and with (B) an induced drift. The top x-axis represents the time after the “GRE-2TE” pre-scan was acquired and the bottom x-axis the frequency at which the saturation pulses were applied at the time instant when each B_0 sample was determined. Differences in MTR_{asym} curves among B_0-correction methods under stable (C) and drifted (D) conditions are shown in the bottom row. The proposed methods CEST-GRE-2TE (light blue), CEST-GRE-1TE (green) and NAV-EPI-2TE (purple) succeeded to track and correct the induced drift $\delta B_0(t)$.

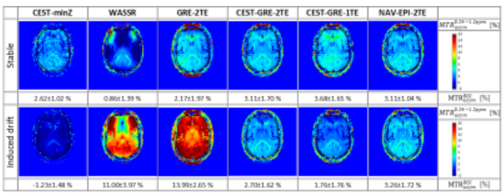

FIG. 3: Effect on the MTR_{asym} maps of a linear induced frequency drift for volunteer V2. The top row shows color-coded maps for the different correction methods in the absence of drifts, the bottom row depicts maps in which there was a ~4Hz/min drift. The static method CEST-minZ overestimated B_0, resulting in decreased map values, while WASSR and GRE-2TE show the opposite effect, since both scans took place before the field drift was applied. Among the dynamic methods, NAV-EPI-2TE compensates this drift most efficiently, providing the closest values within the delineated ROI (in black) between acquisitions, being closely followed by CEST-GRE-2TE.

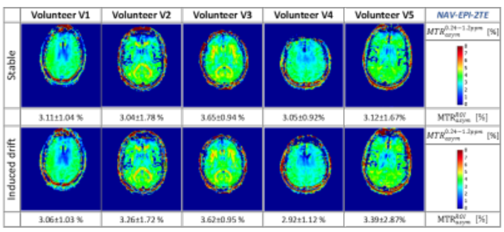

FIG. 4: Comparison of the correction performance of the proposed dynamic method NAV-EPI-2TE for all subjects (V1-V5): B_0-corrected maps in the absence (top row) and in the presence (bottom row) of the induced B_0 drift during the CEST measurement. A ROI along each volunteer’s brain border was manually drawn (delineated in black) and the MTR_{asym} mean ± standard deviation values within this ROI are shown at the bottom of each map. The MTR_{asym} maps are highly consistent between the CEST scans with and without the induced frequency drift in all cases.

Proc. Intl. Soc. Mag. Reson. Med. 27 (2019)
5007